

See discussions, stats, and author profiles for this publication at: <https://www.researchgate.net/publication/7196179>

Transfer RNAs: Electrostatic Patterns and an Early Stage of Recognition by Synthetases and Elongation Factor EF-Tu

ARTICLE in BIOCHEMISTRY · MAY 2006

Impact Factor: 3.02 · DOI: 10.1021/bi0516733 · Source: PubMed

CITATIONS

5

READS

11

5 AUTHORS, INCLUDING:



[Victor V. Ivanov](#)

Joint Institute for Nuclear Research

214 PUBLICATIONS 1,328 CITATIONS

[SEE PROFILE](#)



[Victor S Sivozhelezov](#)

Russian Academy of Sciences

65 PUBLICATIONS 405 CITATIONS

[SEE PROFILE](#)

Transfer RNAs: Electrostatic Patterns and an Early Stage of Recognition by Synthetases and Elongation Factor EF-Tu

Robert V. Polozov,^{*,†} Mikhail Montrel,[†] Victor V. Ivanov,^{‡,§} Yuri Melnikov,[§] and Victor S. Sivozhelezov^{*,||,⊥}

Institute for Theoretical and Experimental Biophysics, Moscow region, Puschino 142290, Russia, Laboratory of Information Technologies, Joint Institute for Nuclear Research 141980, Dubna, Russia, International Solvay Institutes for Physics and Chemistry, CP-231, ULB, Boulevard du Triomphe 1050, Brussels, Belgium, Nanoworld Institute, University of Genoa, 30 Corso Europa, Genoa 16132 Italy, and Institute of Cell Biophysics, Moscow region, Puschino 142290, Russia

Received August 23, 2005; Revised Manuscript Received February 12, 2006

ABSTRACT: Distributions of phosphate backbone-produced electrostatic potentials around several tRNAs were calculated by solving the nonlinear Poisson–Boltzmann equation. The tRNAs were either free or bound to the proteins involved in translation: aminoacyl-tRNA and elongation factor EF-Tu. We identified several regions of strong negative potential related to typical structural patterns of tRNA and invariant throughout the tRNAs. The patterns are conserved upon binding of tRNAs to the synthetase and the EF-Tu. Variation of tRNA charge in our theoretical calculations of electrostatic potential-mediated pK shifts of pH-dependent labels attached to tRNA, compared to experimentally observed pK shifts for those labels, shows that the total charge of tRNA is large, within the interval of –40 to –70 proton charges. The electrostatic field of tRNA is sufficient to cause ionization of histidine residues of ARSase, causing additional free energy of ARSase–tRNA interaction of at least several kcal/mol. This may discriminate proteins with respect to the particular tRNA at large distances. Two types of tRNA–protein electrostatic recognition mechanisms are discussed. One, more specific, involves charges induced on protein by the large electrostatic potential of tRNA, while the other, less specific, does not involve induced charges.

The function of tRNA¹ is amino acid delivery to the ribosome to be used in translation, that is, mRNA-directed synthesis of the polypeptide chain (*1*). Beside tRNAs, initiation factors IF-1, IF-2, and IF-3, release factor RF-3, ribosome, and amino acids, the following components participate in translation: (1) mRNA, (2) elongation factors EF-Tu and EF-G, and (3) aminoacyl-tRNA synthetases (ARSase).

Details of the well-known scenario of the elongation cycle reviewed in ref 2 point to the existence of at least two different types of molecular recognition in this process: codon–anticodon and ARSase–tRNA. The specificity of the former is ensured by hydrogen bonding between complementary nucleic bases, and details of both elongation in general (*3*) and peptide bond formation in particular (*4*) are well-studied. However, the nature of the specificity of the ARSase–tRNA recognition is not so clear despite of its

obvious importance for correct translation. In prokaryotes, each amino acid has its own unique tRNA and ARSase. However, the elongation factor EF-Tu is not specific to amino acid even though some specificity was noted among noncognate aa/tRNA complexes (*5*).

In this study, we put forward a long-distance mechanism of tRNA–ARSase and tRNA–EF-Tu recognition based on electrostatic potentials of tRNA, as a part of a hierarchical mechanism of tRNA–protein recognition.

The concept of hierarchical recognition was initially introduced with respect to protein–DNA recognition process according to which it involved at least three stages (*6*). The first was the nonspecific binding of protein to the nucleic acid driven by the electrostatic complementarity of contacting surfaces between the nucleic acid and the protein (*7*) (the proteins in our case being the ARSase and EF-Tu). The second step, one-dimensional diffusion of a protein along the DNA chain (*8–10*), is unlikely to be valid for tRNA since tRNA has a complex shape and smaller dimensions. The next stage is the formation of more extensive contacts between the nucleic acid and the protein, which occurs when the target site has already been located by the protein along the DNA chain in the case of DNA, or by the tRNA relative to the ARSase and the ribosome in our case.

Studies of electrostatic potentials of tRNA were originated by Pullman and co-workers (*11*) who used a quantum chemistry approach to calculate electrostatic potential of tRNA backbone and nitrogenous bases in vacuo. In more recent studies, electrostatic potential was calculated in solution by solving the Poisson–Boltzmann equation. Honig

* Corresponding authors. For V.S.S.: phone, +39-010-35338203; fax, +39-010-35338215; e-mail, vsivo@nwi.unige.it. For R.V.P.: phone, +7-0967-739155; fax, +7-0967-330509; e-mail, polrob@iteb.ru.

[†] Institute for Theoretical and Experimental Biophysics.

[‡] Joint Institute for Nuclear Research.

[§] International Solvay Institutes for Physics and Chemistry.

^{||} University of Genoa.

[⊥] Institute of Cell Biophysics.

¹ Abbreviations: tRNA, transfer RNA; EF-Tu, elongation factor Tu; ARSase, aminoacyl-tRNA synthetase; IF-1, IF-2, IF-3, initiation factors 1, 2, 3; RF-3, release factor 3; EF-G, elongation factor G; DNA, deoxyribonucleic acid; RNA, ribonucleic acid; 3D, three-dimensional; tRNA^{Phe}, phenylalanyl tRNA; tRNA^{Asp}, aspartyl tRNA; tRNA^{Ser}, seryl tRNA; tRNA^{Thr}, threonyl tRNA; tRNA^{Arg}, arginyl tRNA; aa, amino acid.

and co-workers considered the electrostatic potential of the anticodon loop of tRNA (12) highlighting the differences between the initiator and the elongator tRNA, and also focused on the differences between types of structures found in RNAs (13) with tRNA considered among those structures together with the pseudoknot and the tetraloop. The latter study established that the features of RNA determining its function could not be derived from the molecular structure of RNAs alone, but required calculation of electrostatic fields.

Specificity of tRNA–protein recognition is so far an unresolved issue. It is believed that the recognition specificity is determined by 3D structures of interacting molecules, and the recognition itself occurs upon immediate contact of the molecules at distances close to van der Waals radii. In ref 14, the tRNA–synthetase interaction was treated in the assumption that tRNA is a point charge while the specificity is determined by steering of tRNA by the unique electric field of the synthetase. While agreeing with this approach in terms of electrostatic nature of long-range recognition, we consider an alternative approach in which ionization of histidine residues of the ARSase is induced by the electric field of tRNA.

MATERIALS AND METHODS

We have calculated distributions of electrostatic potentials around the three elongator tRNAs with 3D structures of the free (not protein-bound) form: crystallographic structures of tRNA^{Phe}, tRNA^{Asp}, and the theoretical model of tRNA^{Ser}.

Atomic coordinates were taken from the Protein Data Bank (<http://www.rcsb.org/pdb>). The databank entries used were 4tna for free tRNA^{Phe}, 1ttt for tRNA^{Phe} bound to EF-Tu, 3tra for free tRNA^{Asp}, 1asy for tRNA^{Asp} bound to the ARSase, 1ser for tRNA^{Ser}, and 1eiy for the ARSase.

Electrostatic potentials were calculated by solving the Poisson–Boltzmann equation, as specified in ref 15. This equation relates the electric potential φ with the charge distribution. Its left-hand part contains the sought potential and the dielectric constant ϵ assumed to be 2 inside the protein and 80 outside the protein or tRNA thus allowing for the dielectric boundary, and the right-hand part contains the charge distribution of the protein molecule and the mobile charges of the solution resulting from added salt. The tRNA charges are approximated by point charges placed at the atomic coordinates and include only the phosphate charges, considering that phosphate groups dominate the electrostatic fields of nucleic acids at large distances, which was evident from the start of nucleic acid electrostatic research. The latter assumption was also confirmed in ref 13 exemplified by tetraloop RNA, and we confirm it in this study using phenylalanine tRNA. Therefore, charge assignment for tRNA calculations was limited to phosphate groups, based on the AMBER force field, AMBER99 parameter set, and normalized so as to maintain the –1.0 charge per nucleotide. This limitation was also verified by comparing the results to those for the *Escherichia coli* tRNA^{Phe} molecule, with charges assigned to each atom of the tRNA. For calculations of the synthetases, full atomic charges were assigned according to the same force field and parameter set, in two variants: with the histidine residues completely charged (+1.0) or completely uncharged.

The mobile ions are considered to be Boltzmann-distributed over electrostatic free energy, so $\exp(\varphi)$ appears

in the right-hand side (nonlinear Poisson–Boltzmann equation). Taylor series expansion over the potential and truncation leads to the linearized Poisson–Boltzmann equation. The calculation parameters are concentrations and charges of ions. We assume a 1:1 valent electrolyte at physiological 150 mM concentration.

To solve the Poisson–Boltzmann equation, we apply iterations with respect to φ , which leads to a linear problem at each iteration step. Its solution is sought with finite-difference multigrid method (for detailed discussion, see, e.g., ref 16) using a sequence of nested finite difference rectangular grids. The macromolecule is thus immersed in grids containing $160 \times 160 \times 160$ points for the finest grid, so that the interval between grid points is less than 1 Å. The analytical solution available when ϵ is constant, known as the Coulomb–Debye formula, is used as the first approximation, as well as to establish the boundary conditions at the parallelepiped's outside faces. Such boundary conditions implicitly assume excess electrolyte.

We used the nonlinear Poisson–Boltzmann equation instead of its linearized variant to calculate the tRNA's electrostatic potential because the tRNA surface is strongly curved and highly charged. For tRNAs, the calculated electrostatic potential was visualized as the equipotential surface ($-5 k_B T/q$ units, where q is the proton charge). For both tRNAs and ARSases, potentials were mapped onto the surface 5.5 Å away from the van der Waals surface, and color coded from –10 to 0 $k_B T/q$ units (see Legend to Figure 1). The choice of this distance for potential mapping is dictated by the facts that (1) at this distance away from the van der Waals surface, the surface is approximately 7 Å away from the charges contributing to the potential and (2) that distance equals the so-called Bjorrrum length at which the interaction energy between two unit charges in water is $k_B T$. At smaller distances, electronic fluctuations and correlations (17) lead to breakdown of the point charge model used herein. At larger distances, energy of electrostatic interaction becomes comparable to that of the thermal motion. We compared electrostatic potentials by solving the linear and nonlinear variants of the Poisson–Boltzmann equation and found that the difference is significant, from 0.2 to 1 $k_B T/q$ at the specified equidistant surface (data not shown).

Applicability of the Poisson–Boltzmann equation, even in the nonlinear variant, to electrostatic calculations of nucleic acids has been open to discussion for quite a while, the discussion having been caused mostly by the theoretically predicted and experimentally observed effect of counterion condensation (18, 19 and references therein) or counterion retention (20) around charged bodies. This effect may lead to inaccuracies in Poisson–Boltzmann calculations. The extent of inaccuracies is determined by the magnitude of interionic correlations in counterion distribution near the polyion surface, which depends on many factors including the magnitude of polyion charge and the pattern of its distribution over the polyion molecular surface, as well as shape and curvature of that surface. Combined action of these factors may also cause irregularities in the electric field of the polyion. As follows from the estimates (17, 21), substantial errors in Poisson–Boltzmann calculations may result only in the actual region of the condensation, that is, in the immediate vicinity of the polyion's molecular boundary. This is another reason we selected the surface for electric

potential mapping as far as 5.5 Å away from the molecular surface, to avoid the short-distance errors.

Besides, the geometry of tRNA is intermediate between that of a sphere and a cylinder. The condensation effects in the asymptotic infinite-dilution case were shown to be the most pronounced for a plane, less significant for a cylinder, and totally absent for a sphere (22, 23). The same trend seems to be preserved for the excess electrolyte case. Indeed, recent calculations (24) show that the same surface potential requires different levels of surface charge density for planar, cylindrical, and spherical surfaces, in the order spherical surface > cylindrical surface > planar surface.

RESULTS

Contributions of Backbone Charges and Nitrogenous Bases to the Electrostatic Potential. To compare contributions of the phosphate backbone and the nitrogenous bases, we calculated the electrostatic potential around the *E. coli* tRNA^{Phe} molecule, with charges assigned either to each atom of the tRNA or only to the phosphate atoms. The patterns remained practically the same, in the interval of potential values of $-10 k_B T/q$ to 0 (data not shown). Thus, at given distances and for the given equipotential levels, only the charges of the phosphates contribute to the electrostatic potentials, while charges of the nitrogenous bases and sugar rings can be ignored. Consequently, the unique distribution of electrostatic field around irregularly shaped nucleic acids is dominated by the phosphate charges, while its specific properties are determined by the sequence-dependent spatial arrangement of nucleic acid strands. This distribution may determine the progress of the first protein–nucleic acid recognition stage, at distances about 10 Å.

Overall Distribution of Neutral Potential. Since tRNA has a strongly charged phosphate backbone, the electrostatic potential resulting from it is mostly negative, with only an occasional spot of the almost neutral potential. Such neutral spots are observed near the anticodon loop and the acceptor end. At these sites, nitrogenous bases are exposed to the solvent, while the charged phosphate groups are screened by the nitrogenous bases so their contribution to the electrostatic potential becomes negligible. The almost neutral potential is observed near the TψC loop, obviously caused by screening resulting from the convex shape of the dielectric interface. Note that the serine tRNA, compared to other considered tRNAs, has an additional area of the almost neutral potential near the variable loop (vertex of the “L”) corresponding to the position of the extra bases in that loop located about 10 bases downstream from the anticodon loop. It is those extra bases that cause additional screening.

These effects are also reflected in cavities observed in the equipotential surface. Importantly, these cavities appear even when the nitrogenous base charges were ignored, and we show that they are augmented if nitrogenous bases are taken into account. This agrees with results of ref 13 where charges of the bases were found to be only partly responsible for cavities of equipotential surfaces around RNAs. Earlier data (12) indicate that the cavity at the anticodon loop region is not directly caused by charges of the bases but instead is a combination of two effects: dielectric boundary and local conformation.

Regions of Negative Potentials. In all five tRNA structures considered herein, the most negative potential is located in

the following regions (spots, top parts of Figures 1–5): in the front view, a large, very strong spot at the center of the molecule (Spot 1), a smaller spot (Spot 2) near the anticodon loop, and a small spot near the acceptor end (Spot 3); at the backside, a spot between the TψC stem and the acceptor stem (Spot 4), and another spot near the D loop (Spot 5). In tRNA^{Phe}, both free and elongation factor-bound, Spot 1 is divided into two spots by a region of weak potential, because bases 44–46 in the variable loop protrude more in tRNA^{Phe} than in tRNA^{Asp} (Figures 1 and 2, left panels).

Binding of tRNA to Proteins Affects Invariant Regions of Electrostatic Potential. In the free tRNA^{Ser}, Spot 1 is shifted about 5 Å in the direction of the anticodon loop with respect to its position in the remaining tRNAs. This difference is readily explained by structural features of tRNAs near bases 44–46. Indeed, it is at this region of primary tRNA structure where the additional loop is inserted in tRNA^{Ser}.

As seen from comparing Figures 2 and 4 to Figures 2 and 3, upon binding of tRNA to the synthetase, intensities of all the five (negative) spots of tRNA^{Asp} decrease, and so do the areas occupied by them. The overall shape of the tRNA^{Asp} and its electrostatic field reflected by both equidistant and equipotential surface drastically changes upon binding to the synthetase. Indeed, both regions decrease about 10% in size in the direction between the anticodon loop and the acceptor end. In contrast, upon binding to the EF-Tu, the intensities of Spots 1, 4, and 5 of tRNA^{Phe} decrease, but the area occupied by them remains practically unchanged, while Spots 2 and 3 remain almost unchanged in both intensities and occupied areas. The overall shape of the tRNA^{Phe} and its electric field remains unchanged upon binding to the synthetase. Therefore, for both tRNA^{Phe} and tRNA^{Asp}, a decrease in intensity of the electric field is observed, but the decrease is less pronounced in the case of EF-Tu. Besides, apparent local details of this decrease differ between the synthetase and the EF-Tu.

Validation of the Large Total tRNA Charge. We attempted to verify the high value of tRNA total charge by comparing our results to the available experimental data (25) in which pK shifts for a pH-dependent fluorescent label attached to different regions of the tRNA to pK shifts were reported. We calculated those pK shifts for several values of total tRNA charge, varying it from -10 to -76 q. The shift of local pK by electrostatic field follows the equation $\Delta pK = -0.434\Delta\phi$, where $\Delta\phi$ (expressed in $k_B T/q$ units) is the additional electrostatic potential, in our case the potential of tRNA. The fluorescein-based labels used in ref 25 have the titratable group at about 9 Å distance from the point of attachment to the tRNA and, therefore, at about 7.5 Å distance from the tRNA’s molecular surface. Accordingly, we calculated the phenylalanine tRNA’s electrostatic potential for the salt concentrations used in that study, which was 100 mM NaCl and 0.2 mM MgCl₂, and mapped it on the surface 7.5 Å away from tRNA’s molecular surface. Since the range of ΔpK shifts experimentally observed (25) was 0.24–1.18, we color-coded the mapped potential so that orange corresponded to ΔpK of 1 pK unit, yellow to 0.5, and green to 0. Three values of tRNA total charge were considered, which were -10 , -40 , and -76 q. For the total tRNA charge of -10 q, the surface was uniformly green so the predicted pK shift was negligible (data not shown). For the total tRNA charge of -40 q (Figure 6, left panels), the

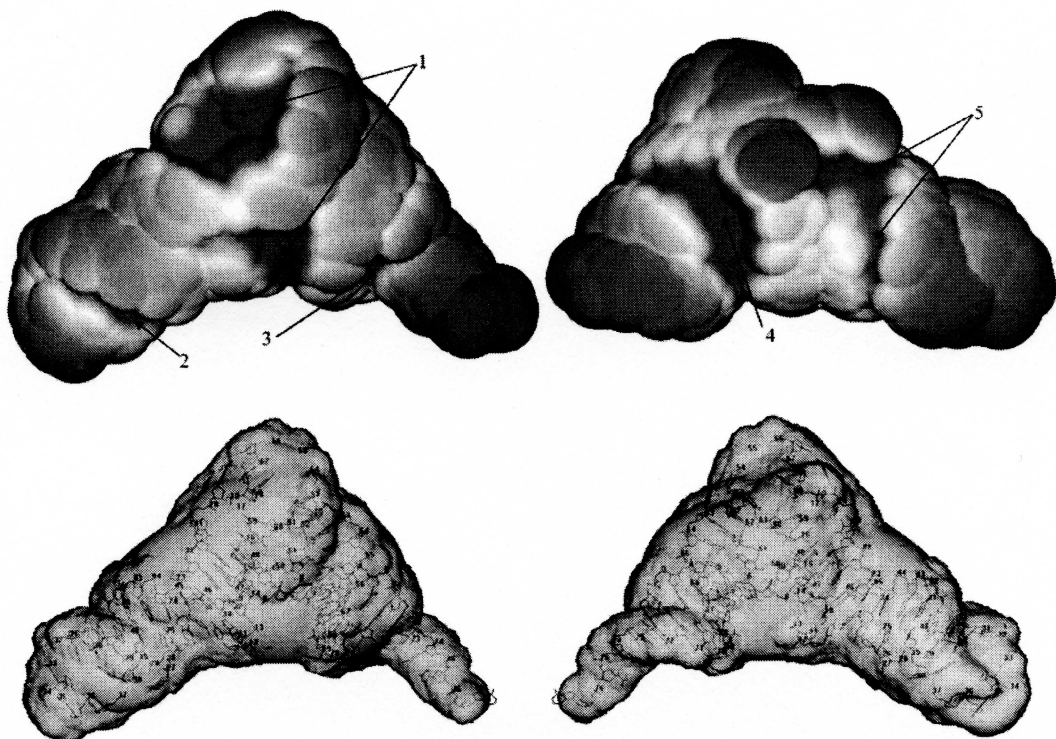


FIGURE 1: Distribution of electrostatic potential around free tRNA^{Phe}. (Top panels) Potential mapped at a surface equidistant (5.5 Å) from van der Waals surface: red, $-10 k_B T/q$; white, $-5 k_B T/q$; blue, 0. Left panel, front view; right panel, back view. (Bottom panels) Equipotential surface of $-5 k_B T/q$. Left panel, front view; right panel, back view.

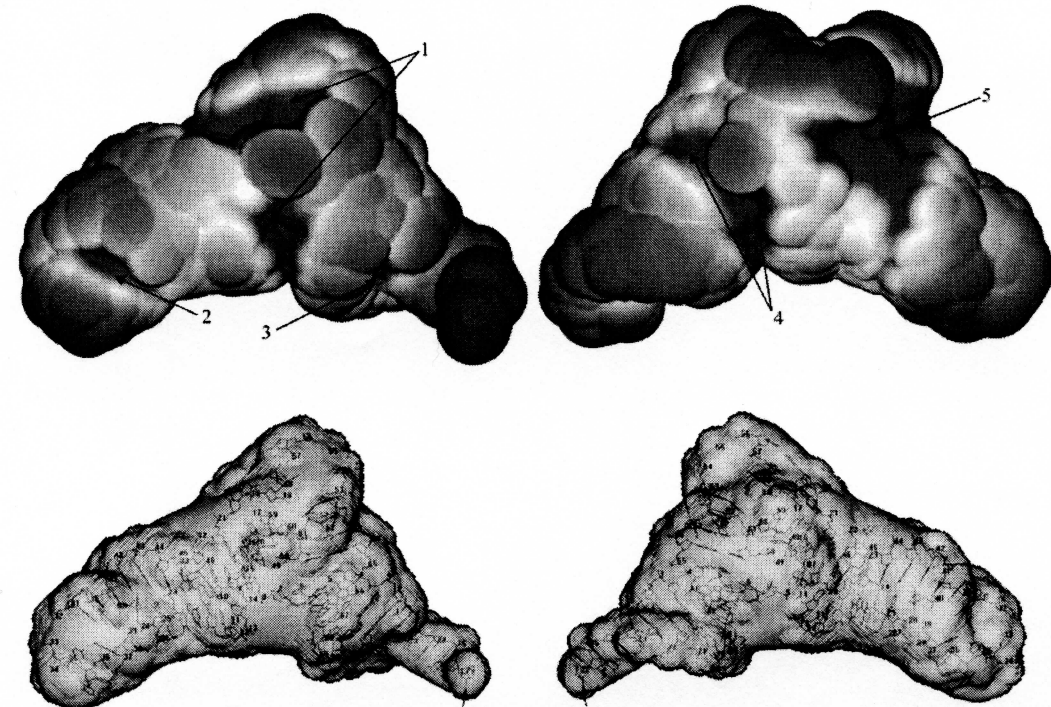


FIGURE 2: Distribution of electrostatic potential around tRNA^{Phe} bound to elongation factor (EF-TU). (Top panels) Potential mapped at a surface equidistant (5.5 Å) from van der Waals surface: red, $-10 k_B T/q$; white, $-5 k_B T/q$; blue, 0. Left panel, front view; right panel, back view. (Bottom panels) Equipotential surface of $-5 k_B T/q$. Left panel, front view; right panel, back view.

surface was also mostly green, with only occasional spots of orange (shift by 1 pK unit), and several fair-sized spots of yellow (shift by 0.5 pK unit). For the -76 q total tRNA

charge (Figure 6, right panel), more than half of the surface is orange (shift by 1.0 or more pK unit), in qualitative agreement with experimental results of ref 25. This com-

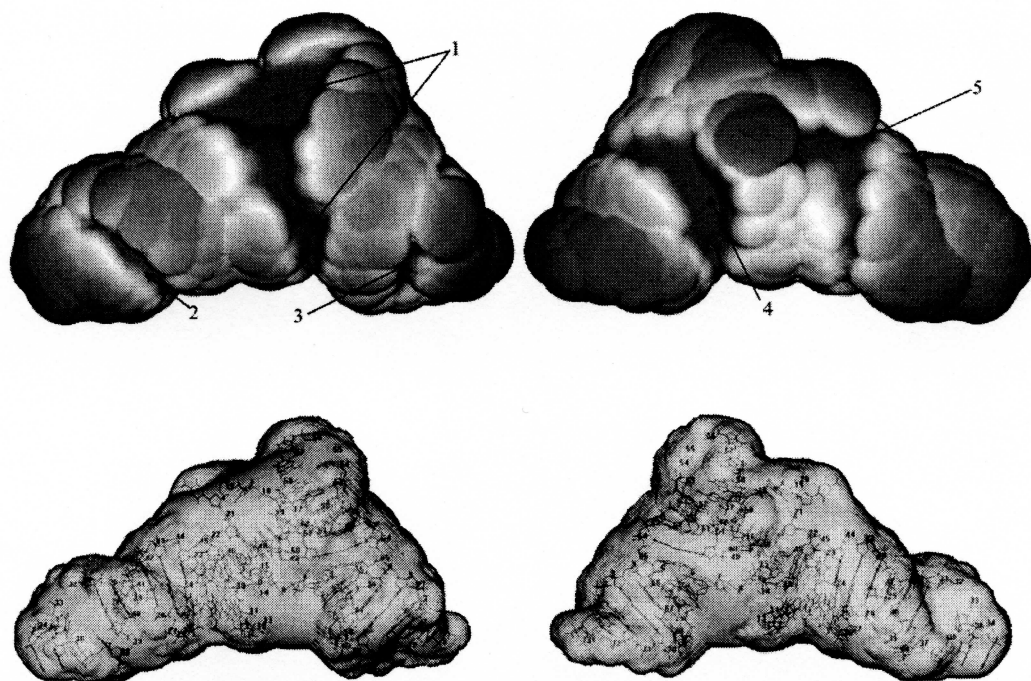


FIGURE 3: Distribution of electrostatic potential around free tRNA^{Asp}. (Top panels) Potential mapped at a surface equidistant (5.5 Å) from van der Waals surface: red, $-10 k_B T/q$; white, $-5 k_B T/q$; blue, 0. Left panel, front view; right panel, back view. (Bottom panels) Equipotential surface of $-5 k_B T/q$. Left panel, front view; right panel, back view.

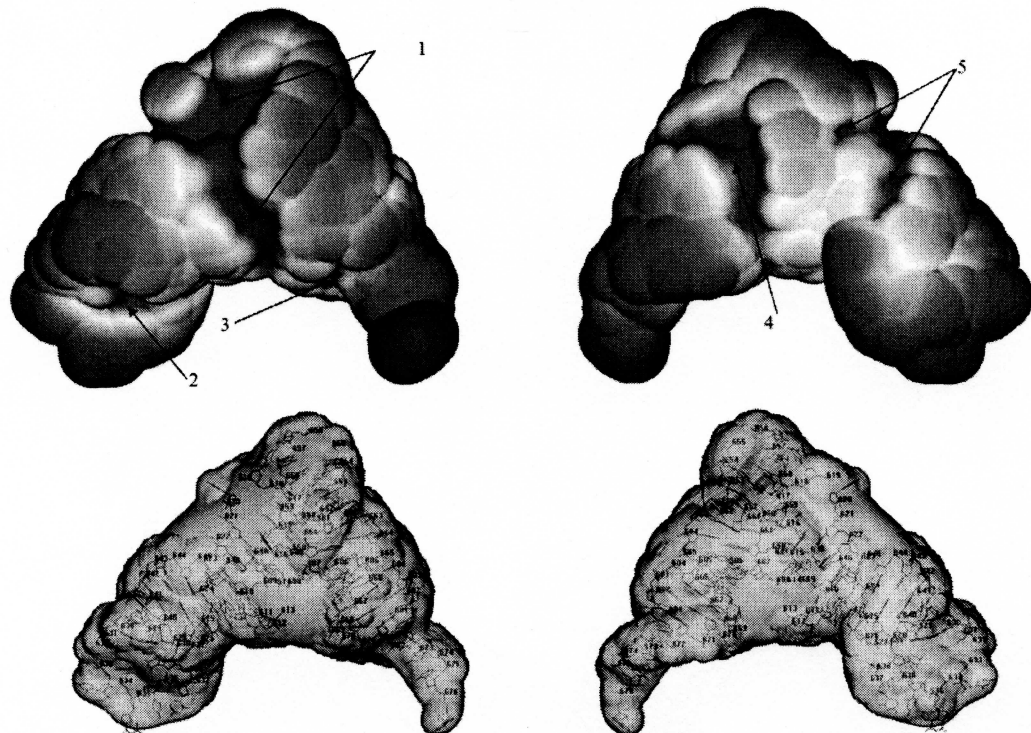


FIGURE 4: Distribution of electrostatic potential around tRNA^{Asp} bound to aspartyl-tRNA synthetase. (Top panels) Potential mapped at a surface equidistant (5.5 Å) from van der Waals surface: red, $-10 k_B T/q$; white, $-5 k_B T/q$; blue, 0. Left panel, front view; right panel, back view. (Bottom panels) Equipotential surface of $-5 k_B T/q$. Left panel, front view; right panel, back view.

parison suggests that the actual overall charge of tRNA should be between -40 and -76 q.

The validity of using pK shifts for estimating the overall charge may be challenged by the fact that the pK shifts

measured for ionizable reagent intercalating in the DNA minor groove is relatively small, 2–2.5 pK units (26). However, later calculations of those pK shifts (27) show that the large Coulombic contribution of phosphate charges to

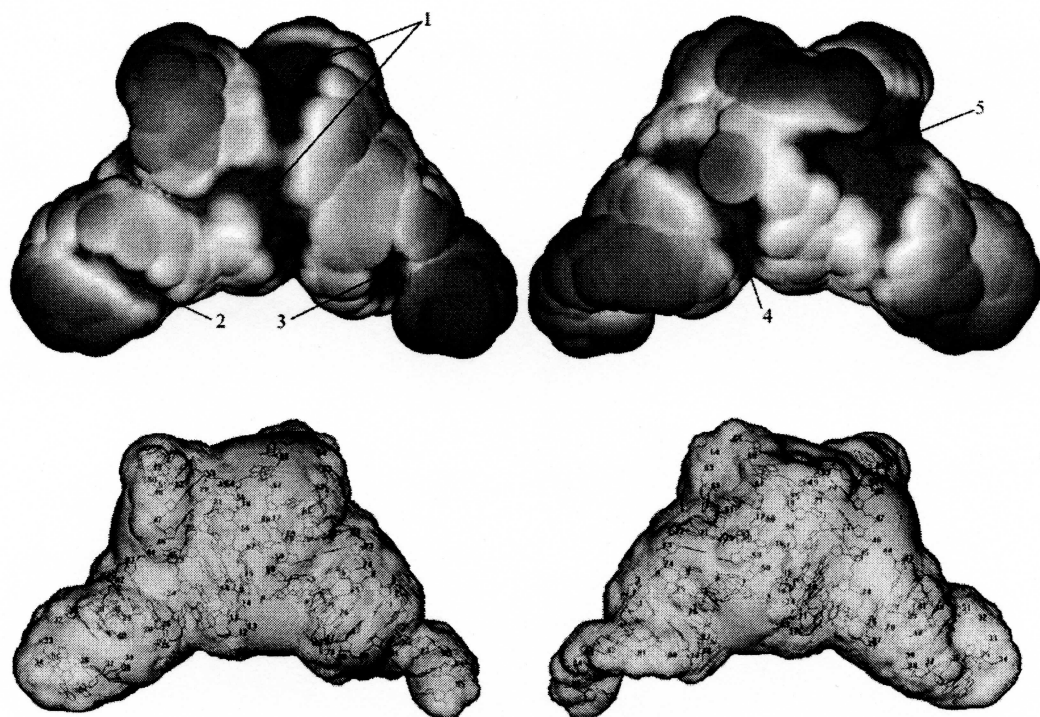


FIGURE 5: Distribution of electrostatic potential around free tRNA^{Ser}. (Top panels) Potential mapped at a surface equidistant (5.5 Å) from van der Waals surface: red, $-10 k_B T/q$; white, $-5 k_B T/q$; blue, 0. Left panel, front view; right panel, back view. (Bottom panels) Equipotential surface of $-5 k_B T/q$. Left panel, front view; right panel, back view.

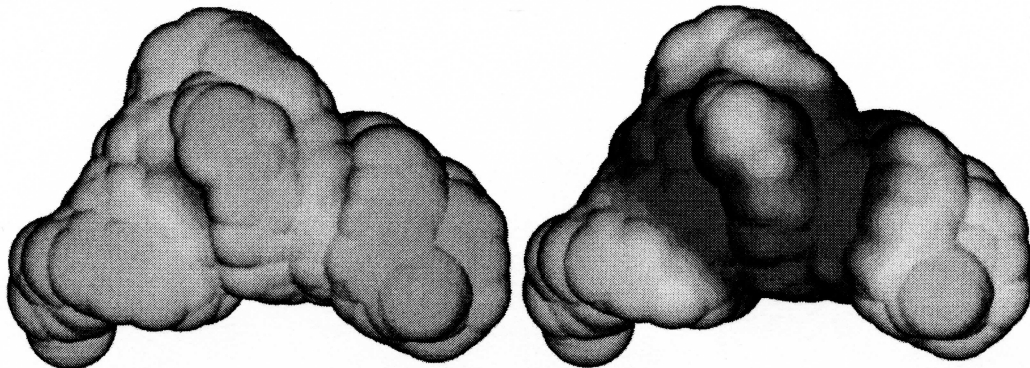


FIGURE 6: Distribution of pK shifts caused by electrostatic field of tRNA^{Phe}. The pK shifts are mapped at a surface equidistant (7.5 Å) from van der Waals surface: orange, 1 pK unit; yellow, 0.5 pK unit; green, 0. Left panel, tRNA total charge equals -40 ; right panel, tRNA total charge equals -76 .

pK shifts is considerably compensated by replacement of aqueous media around the titratable site (in absence of DNA) with media containing a dielectric boundary (in the presence of DNA). This compensatory effect manifests only at short (about 2 Å as in ref 27) distances from the nucleic acid surface and is negligible at distances over 5.5 Å since the image charge caused by presence of the dielectric boundary decreases strongly with distance.

Our above conclusion about the high overall tRNA charge is in contrast with the estimates of tRNA total charge from second virial coefficients for diffusivity listed in ref 28, from -10 to -12 q. However, the second virial coefficients actually allow to estimate pairwise interaction energies rather than the total charges, while estimates of the total charges require assumption of geometries of the interacting species (in this case two tRNA molecules). In the above-cited paper,

this geometry was assumed to be spherical, which is very inexact with respect to the tRNA which is actually L-shaped. Therefore, we believe that our conclusions with respect to invariant and variable features of tRNA electrostatic potential, as well as the proposed “induced specificity” mechanism, are sufficiently well-grounded.

DISCUSSION

Structural Origin and Patterns of the Spots of High Electrostatic Potential. In relation to the shapes of the equidistant surface, Spots 1 and 4 belong to the inner surface of the TψC loop. The large potential in those regions is related to the well-known dielectric focusing effect (29), which augments the contribution of charges of the phosphates. Spots 2, 3, and 5 also very probably originate from the dielectric focusing effect since clefts, however small, are

visible in the equidistant surface. However, in contrast to Spots 1 and 4, these three spots are determined by local rather than global structural features of tRNAs. All three spots correspond to narrow parts (knots) between various elements of tRNA secondary structure (bottom parts of Figures 1–5). Particularly, Spot 2 covers the knot between the anticodon loop and the adjacent anticodon stem, and Spot 3 covers the knot between the acceptor end and the adjacent acceptor stem. Spot 5 covers the groove within the anticodon stem. Since those five spots are observed in all the tRNAs we studied, we suggest them to be base-independent invariants of the electrostatic potential distribution around tRNAs. Even though this observation is made using a relatively small number (five) of tRNA structures, the suggested invariants are very likely valid because they are based on highly invariant elements of tRNA structure. This invariant number of spots and topology of strong ($<-5 k_B T/q$ at 150 mM ionic strength and $T = 300$ K) potential spots might be a characteristic property of tRNA comprising an electrostatic “portrait” distinguishing them from other classes of RNAs. In particular, these invariants should be responsible for tRNA–EF-Tu and tRNA–ARSase recognition.

Electrostatic Fields in Protein–tRNA Recognition. Our data indicate that reduction of long-range electrostatic effects upon tRNA binding to the protein should be caused by conformational changes that are different for the synthetase and for the elongation factor. In the case of the synthetase, all of the spots of strong negative potential are affected with respect to both the intensity and the occupied area, suggesting that the decreased phosphate contribution is accompanied by conformational changes in the structure of tRNA^{Asp} upon binding to the synthetase.

In contrast, the spots are much less affected by EF-Tu binding. Considering that long-range electrostatic patterns found herein should be invariant over different tRNAs, long-distance electrostatic effects should not contribute to specificity of tRNA binding to EF-Tu. This conclusion contradicts the data on interaction of EF-Tu with noncognate (misacylated) tRNA–amino acid conjugates (5) where thermodynamic constants for EF-Tu–tRNA binding were found to vary over 2 orders of magnitude over the 21 studied tRNAs. However, it was also established that the difference in thermodynamic constants reflects the difference in unimolecular dissociation constants, while the bimolecular association constants did not depend on the tRNA type (30). Apparently, the long-range, early-stage electrostatic effects considered herein should affect the bimolecular association constant, while the unimolecular dissociation constant should be governed by closer-range interactions in which electrostatic interactions are only one, and possibly the least significant, of several contributing factors. Therefore, electrostatic contribution to tRNA–EF-Tu interaction is stronger in the association than in dissociation, thereby favoring dissociation after the function of tRNA–EF-Tu recognition has been completed.

With respect to the highly specific tRNA–ARSase recognition, the decrease of the distance between the anticodon loop and the acceptor end seen from both the equipotential surface and the tRNA^{Asp} structure may also have biological significance. Unlike the contact of seryl-tRNA synthetase with tRNA^{Ser}, aspartyl-tRNA synthetase contacts tRNA^{Asp} via the ends of both the acceptor end and the anticodon loop

(31). Such diversity reflects the known fact that ARSases are highly modular proteins selecting their cognate tRNAs via recognition of several specific regions of tRNA, with each tRNA region corresponding to a separate domain of ARSase and tRNA co-evolving with its cognate ARSase (32).

Significance of the High Total Charge of tRNA. The important point which remains open to discussion is that of the biological significance of tRNAs’ high total charge. It has been shown earlier (13) that tRNAs, unlike other nucleic acids, are closer to proteins in their molecular topology. The maximum overall charge born by proteins, however, is exemplified by ferredoxins bearing the charge of about -20 q for about 60 amino acids (33), or cytochromes C with about $+15$ q for about 100 amino acids (34), which is well below the $-n$ q for the n -nucleotide tRNAs.

One suggestion for the functional role of high tRNA’s total charge has been put forward in ref 14, where this high charge has been proposed to guide the tRNA to its destination on the surface of the synthetase. Following the calculation of electrostatic potential distribution around the synthetase and by visualizing the equipotential surface of $\pm 0.01 k_B T/q$, the authors suggest that the difference in energy (equal to $\pm 0.01 k_B T/q \times 70$ q = $\pm 0.7 k_B T$) is sufficient to ensure the electrostatic guiding. We have reproduced this result using our methods (Figure 7, left panel, cf. Figure 1A of ref 14) and parameter values used in the quoted calculation. These parameter values, particularly the default atomic charge assignment of AMBER force field, imply that histidines are completely uncharged, and we had to make the same assumption to reproduce the result. However, there is no reason to assume complete absence of total charge on histidine residues considering that, under physiological conditions (pH 7), histidines (pK ranging from 5.5 to 8 in different proteins) are likely to bear a fractional charge. We found that the shape of the equipotential surface changes considerably if histidines are charged (Figure 7, right panel). Particularly, the positive equipotential surface that was assumed (14) to guide the tRNA to the active site of the synthetase has increased so much that its guiding role seems to be open for discussion.

Here, we are putting forward an alternative explanation of physiological significance of large total charge of tRNA, assuming that it may change the ionization state of the synthetase in such a way that the histidine residues change their charge from near-zero to near unity. We have shown that the equipotential surface of $-5 k_B T/q$ protrudes away from tRNA surface. The effects can be roughly estimated following the known Henderson–Hasselbalch equation, which is written for weak bases such as the histidine side chain as $\log(\alpha/(1 - \alpha)) = pK - pH$, where α is the ionization ratio (for histidines, it is also the amino acid residue charge in elementary units). We assume the physiological pH value to be 7.0, and use the above-quoted equation $\Delta pK = -0.434\Delta\phi$. For the extreme case $pK = 5.5$, we obtain $\alpha = 0.03$ if $\Delta\phi = 0$ (in absence of tRNA) and $\alpha = 0.91$ if $\Delta\phi = 5 k_B T/q$. This means that the electric potential of tRNA may change the histidines of synthetase from uncharged to an almost completely charged state, even for the histidines least prone to charging. For the other extreme case, $pK = 8.0$, $\alpha = 0.91$ even if $\Delta\phi = 0$ (in absence of tRNA). These estimates suggest that the approaching tRNA may induce additional charges on the synthetase. The

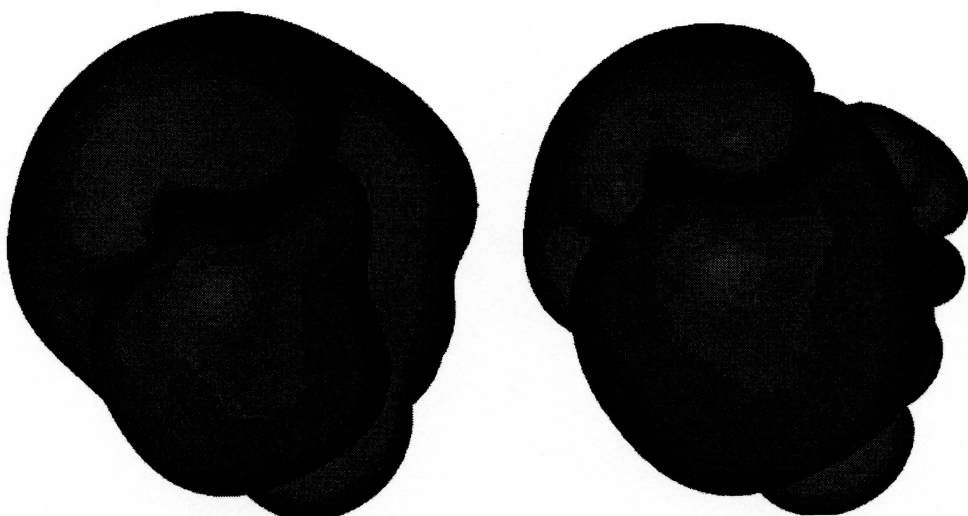


FIGURE 7: Distribution of electrostatic potential around arginyl-tRNA synthetase. Equipotential surfaces are shown for $+0.01 k_B T/q$ (blue) and $-0.01 k_B T/q$ (red). Left panel, histidines uncharged as in ref 14; right panel, histidines charged.

amplitude of this effect can be evaluated by considering the total charges of the synthetases quoted in ref 14: depending on histidine ionization, the total charge per one tRNA molecule will vary from -1 to -27 q for tRNA^{Phe} synthetase, from $+6$ to -17 q for tRNA^{Thr} synthetase, and from $+8$ to -6 q for tRNA^{Arg} synthetase.

As seen from Figures 1–5, the linear dimension of regions of $-5 k_B T/q$ equipotential surfaces outside the tRNA molecules is about 15 Å. The numbers of ionizable histidines in the seryl, aspartyl, and phenylalanyl ARSases able to be simultaneously covered by those regions are 2, 4, and 3, respectively. Hence, the induced charges may alter the binding free energy by about 6, 12, and 8 kcal/mol respectively. Thus, switching of histidines from uncharged to the charged state under action of the tRNA electric field could lead to increased specificity of the tRNA–synthetase interaction.

Electrostatic Mechanisms of Recognition and Limits of Their Applicability. Our data suggest two possible mechanisms of electrostatic recognition: one follows directly from the obtained patterns of tRNA electrostatic potential, while the other, more specific, is the “induced specificity” caused by ionization of protein side chains in the large electrostatic field of tRNA. In both cases, the long-range nature of this mechanism implies that its details cannot be captured by either the 3D structures of the partners or even the structures of their complexes. This factor of recognition is quasi-independent of 3D structure.

As follows from our data, recognition of EF-Tu by tRNA upon association may be based on the electrostatic pattern of tRNA alone, which is related to the fact that the EF-Tu–tRNAs complex is formed outside the ribosome. In contrast, dissociation of the tRNA–EF-Tu complex is more likely determined by its interactions with ribosomal proteins and RNAs rather than tRNAs.

The earliest stages of tRNA–ARSase recognition involve both the distribution of negative-potential spots (electrostatic portrait) of tRNA and ability of histidine residues of ARSases to become protonated in the field of tRNA. Thus, the specificity of tRNA–ARSase recognition originates from the interaction of tRNA with the highly specific pattern of

ARSase induced by protonation of ARSase histidine residues in the weakly specific electric field of tRNA. After the specific complex is formed, the induced charge pattern on ARSase may be varied, for example, by varying the local pH and/or amino acid binding and thus facilitate ARSase dissociation from the tRNA. Dissociation may also be favored by smaller electrostatic potential of tRNA in the synthetase-bound form compared to its free form.

Since this recognition mechanism requires at least two factors, (1) very large overall charge of one of the partners and (2) presence of many ionizable amino acid side chains in the other partner, limits of its applicability should be rather narrow under normal physiological conditions (particularly neutral pH), although it may operate under pathological conditions.

The specific but still long-range tRNA–ARSase recognition mechanism may be required since amino acid attachment to tRNA (loading) is a very important control point of translation and may be specific to translation rather than transcription. Specificity, even at the early stage of recognition, is particularly important in the process of loading, considering that, once the amino acid is delivered to the ribosome, it can be inserted into the growing protein chain regardless of the identity of tRNA that delivered it (37). In contrast, atomic-scale recognition during transcription is reached only upon immediate contact of DNA and proteins, for example, DNA/RNA polymerases and regulatory proteins. There are two physical factors responsible for the difference between tRNA–protein and DNA–protein recognition. One of those is the globular-like shape of tRNA instead of quasi-linear shape of DNA. The other is the uncompensated charge of tRNA shown herein, instead of condensation-screened DNA charge.

Electrostatic effects in tRNA–ARSase and tRNA–EF-Tu recognitions are unlikely to be relevant also to the ternary aa/tRNA/EF-Tu complex within the ribosome, since the ribosome is a complex-shaped multiprotein system containing also the highly charged mRNA molecule. Apparently, the two processes, tRNA–synthetase recognition (part of tRNA loading mechanism) and the ribosome–ternary complex recognition (part of protein biosynthesis mechanism) were

spatially separated in the course of evolution. Besides, if tRNA is within the ribosome, contribution of its charge into the electrostatic potential is difficult to estimate quantitatively, considering also the low resolution of available structural data, for example, only protein alpha carbon atoms and RNA phosphorus atoms are resolved in ref 35. Qualitative estimates are available in ref 36 where they are used to clarify the mechanism of translocation. We consider the tRNA-ARSase and tRNA-EF-Tu complexes before they interact with the ribosome, in the cytoplasm, and do not take presence of the ribosome into consideration. Despite the long-range nature of electrostatic interactions, they are screened in aqueous solutions, so the systems we consider can be treated as almost isolated and independent of ribosomal proteins and RNAs.

Electrostatic fields, and therefore specificity of electrostatic recognition, can be readily controlled by parameters of intracellular or extracellular aqueous media such as ionic strength, pH, or concentrations of ligands able to specifically bind to each recognition partner. Such recognition mechanisms are most likely evolutionarily related and require conservation and evolutionary development of not only sequences and structures of biomolecules, but also shapes of electrostatic, hydrophobic, and stereochemical fields surrounding those biomolecules. Those fields are very difficult to measure and, in many cases, cannot be derived even from atomic-resolution molecular structures. Therefore, computer modeling exemplified by the approach used herein remains a promising method for assessing those fields.

ACKNOWLEDGMENT

The authors are indebted to Dr. Alexander Gorelov, Dr. Anna Panchenko, and Prof. Valery Ivanov for helpful criticism and discussion and Prof. V. G. Kadyshevsky for encouragement and support.

REFERENCES

- Koolman, J., and Rohm, K. H. (1998) *Taschenatlas der Biochemie*, Stuttgart-New York, Georg Thieme Verlag, New York.
- Rodnina, M. V., Gromadski, K. B., Kothe, U., and Wieden, H. J. (2005) Recognition and selection of tRNA in translation, *FEBS Lett.* **579**, 938–942.
- Wintermeyer, W., Peske, F., Beringer, M., Gromadski, K. B., Savelsbergh, A., and Rodnina, M. V. (2004) Mechanisms of elongation on the ribosome: dynamics of a macromolecular machine, *Biochem. Soc. Trans.* **32**, 733–737.
- Rodnina, M. V., Beringer, M., and Bieling, P. (2005) Ten remarks on peptide bond formation on the ribosome, *Biochem. Soc. Trans.* **33**, 493–498.
- Asahara, H., and Uhlenbeck, O. C. (2002) The tRNA specificity of *Thermus thermophilus* EF-Tu, *Proc. Natl. Acad. Sci. U.S.A.* **99**, 3499–3504.
- Ohendorf, D. H., and Matthew, J. B. (1985) Electrostatics and flexibility in protein-DNA interactions, *Adv. Biophys.* **20**, 137–151.
- Fogolari, F., Elcock, A. H., Esposito, G., Viglino, P., Briggs, J. M., and McCammon, J. A. (1997) Electrostatic effects in homeodomain-DNA interactions, *J. Mol. Biol.* **267**, 368–381.
- Hsieh, M., and Brenowitz, M. (1997) Comparison of the DNA association kinetics of the Lac repressor tetramer, its dimeric mutant Lacladi, and the native dimeric Gal repressor, *J. Biol. Chem.* **272**, 22092–22096.
- Jeltsch, A., Wenz, C., Stahl, F., and Pingoud, A. (1996) Linear diffusion of the restriction endonuclease EcoRV on DNA is essential for the in vivo function of the enzyme, *EMBO J.* **15**, 5104–5111.
- Berkhout, B., and van Wamel, J. (1996) Accurate scanning of the BssHII endonuclease in search for its DNA cleavage site, *J. Biol. Chem.* **271**, 1837–1840.
- Lavery, R., Pullman, A., and Pullman, B. (1980) The electrostatic molecular potential of yeast tRNAPhe. (I). The potential due to the phosphate backbone, *Nucleic Acids Res.* **8**, 1061–1079.
- Sharp, K. A., Honig, B., and Harvey, S. C. (1990) Electrical potential of transfer RNAs: codon–anticodon recognition, *Biochemistry* **29**, 340–346.
- Chin, K., Sharp, K. A., Honig, B., and Pyle, A. M. (1999) Calculating the electrostatic properties of RNA provides new insights into molecular interactions and function, *Nat. Struct. Biol.* **6**, 1055–1061.
- Tworowski, D., and Safro, M. (2003) The long-range electrostatic interactions control tRNA–aminoacyl–tRNA synthetase complex formation, *Protein Sci.* **12**, 1247–1251.
- Fedoseyev, A. I., Sivozhelezov, V. S., Purtov, S. V., Petrenko, I. I., and Lazarev, P. I. (1992) Mathematical modelling of 3D protein molecule potential in nonlinear media, *Proceedings of the International Conference "Physique en Herbe-92"*, Marseille, France, pp 222–228.
- Holst, M., Kozack, R. E., Saied, F., and Subramaniam, S. (1994) Treatment of electrostatic effects in proteins: multigrid-based Newton iterative method for solution of the full nonlinear Poisson–Boltzmann equation, *Proteins* **18**, 231–245.
- Netz, R. R., and Orland, H. (2003) Variational charge renormalization in charged systems, *Eur. Phys. J. E* **11**, 301–311.
- Manning, G. S., and Ray, J. (1998) Counterion condensation revisited, *J. Biomol. Struct. Dyn.* **16**, 461–476.
- Manning, G. S. (1978) The molecular theory of polyelectrolyte solutions with applications to the electrostatic properties of polynucleotides, *Q. Rev. Biophys.* **11**, 179–246.
- Lampert, M. A. (1985) The nonlinear Poisson–Boltzmann equation, *Nature* **315**, 159.
- Fixman, M. (1979) The Poisson–Boltzmann equation and its application to polyelectrolytes, *J. Chem. Phys.* **70**, 4995–5005.
- Zimm, B. H., and Le Bret, M. (1983) Counter-ion condensation and system dimensionality, *J. Biomol. Struct. Dyn.* **1**, 461–471.
- Frank-Kamenetskii, M. D., Anshelevich, V. V., and Lukashin, A. V. (1987) Polyelectrolyte model of DNA, *Usp. Fiz. Nauk* **151**, 595–618 (Russian).
- Lin, S. H., Hsu, J. P., Tseng, S., and Chen, C. J. (2005) Analytical expressions for the electrical potential near planar, cylindrical, and spherical surfaces for symmetric electrolytes, *J. Colloid Interface Sci.* **281**, 255–257.
- Friedrich, K., Woolley, P., and Steinhauser, K. G. (1988) Electrostatic potential of macromolecules measured by pK_a shift of a fluorophore. 2. Transfer RNA, *Eur. J. Biochem.* **173**, 233–239.
- Jones, R. L., and Wilson, W. D. (1981) Effect of ionic strength on the pK_a of ligands bound to DNA, *Biopolymers* **20**, 141–154.
- Misra, V. K., and Honig, B. (1995) On the magnitude of the electrostatic contribution to ligand–DNA interactions, *Proc. Natl. Acad. Sci. U.S.A.* **92**, 4691–4695.
- Rhee, K. W., Potts, R. O., Wang, C. C., Fournier, M. J., and Ford, N. C., Jr. (1981) Effects of magnesium and ionic strength on the diffusion and charge properties of several single tRNA species, *Nucleic Acids Res.* **9**, 2411–2420.
- Klapper, I., Hagstrom, R., Fine, R., Sharp, K., and Honig, B. (1986) Focusing of electric fields in the active site of Cu–Zn superoxide dismutase: effects of ionic strength and amino-acid modification, *Proteins* **1**, 47–59.
- Ibba, M., Sever, S., Praetorius-Ibba, M., and Soll, D. (1999) Transfer RNA identity contributes to transition state stabilization during aminoacyl-tRNA synthesis, *Nucleic Acids Res.* **27**, 3631–3637.
- Ruff, M., Krishnaswamy, S., Boeglin, M., Poterszman, A., Mitschler, A., Podjarny, A., Rees, B., Thierry, J. C., and Moras, D. (1991) Class II aminoacyl transfer RNA synthetases: crystal structure of yeast aspartyl-tRNA synthetase complexed with tRNA(Asp), *Science* **252**, 1682–1689.
- Lipman, R. S., and Hou, Y. M. (1998) Aminoacylation of tRNA in the evolution of an aminoacyl-tRNA synthetase, *Proc. Natl. Acad. Sci. U.S.A.* **95**, 13495–13500.
- Brereton, P. S., Maher, M. J., Tregloan, P. A., and Wedd, A. G. (1999) Investigation of the role of surface residues in the ferredoxin from *Clostridium pasteurianum*, *Biochim. Biophys. Acta* **1429**, 307–316.

34. Feinberg, B. A., Ryan, M. D., and Wei, J. F. (1977) Comparative kinetic-ionic strength study of two differently charged cytochrome C: effects are limited to overall charge, *Biochem. Biophys. Res. Commun.* **79**, 769–775.
35. Valle, M., Zavialov, A., Li, W., Stagg, S. M., Sengupta, J., Nielsen, R. C., Nissen, P., Harvey, S. C., Ehrenberg, M., and Frank, J. (2003) Incorporation of aminoacyl-tRNA into the ribosome as seen by cryo-electron microscopy, *Nat. Struct. Biol.* **10**, 899–906.
36. Trylska, J., Konecny, R., Tama, F., Brooks, C. L., III, and McCammon, J. A. (2004) Ribosome motions modulate electrostatic properties, *Biopolymers* **74**, 423–431.
37. Dale, T., and Uhlenbeck, O. C. (2005) Binding of misacylated tRNAs to the ribosomal A site, *RNA* **11**, 1610–1615.

BI0516733